Theoretical model for motility and processivity of two-headed molecular motors

Ryo Kanada and Kazuo Sasaki*
Department of Applied Physics, Tohoku University, Aoba-yama, Sendai 980-8579, Japan
(Received 5 February 2003; published 27 June 2003)

The processive motion of two-headed molecular motors is studied theoretically by introducing a model that takes into account the coordinated motion of the constituent heads and the detachment process of heads from linear molecular tracks. The mean velocity, the mean run length, and the mean run time of the motor along the track are calculated numerically based on the Langevin equation. It turns out that the model, with appropriate choice of model parameters, can explain qualitatively the dependence of these quantities on the external load and adenosin triphosphate concentration observed experimentally for kinesin motors. Furthermore, we discuss how the motility and processivity of the motor are affected by various model parameters, which may be tested by experiments.

DOI: 10.1103/PhysRevE.67.061917 PACS number(s): 87.16.Nn, 87.10.+e, 05.40.−a, 87.17.Aa

I. INTRODUCTION

Kinesin is a motor protein that moves unidirectionally along a one-dimensional polar track called a microtubule, and is responsible for intracellular transport of vesicles and organelles [1,2]. A kinesin motor can translate long distances by hydrolyzing a large number of ATP (adenosin triphosphate) molecules before it dissociates from a microtubule. This property, known as *processivity*, contrasts with the fact that certain motor proteins, such as myosin II in muscle, dissociate from tracks after a single cycle of ATP hydrolysis. In the case of conventional kinesin, it is thought that the processivity is closely related with its two-headed structure: one head remains attached to the microtubule, while the other, detached head, explores for a new site on the track to be attached; hence the molecule can translate in a ''hand-over-hand'' fashion [1,3] or in an ''inchworm'' style [4]. The velocity and the run length have been studied extensively for conventional kinesin by observing the motion of individual motor molecules [5–8].

Various theories have been proposed to explain the experimental results on kinesin motility. They can be grouped into two categories. One approach uses a multistate chemical kinetic description and postulates that the motor steps through a sequence of discrete chemical states [8,9]. Although this phenomenological approach is successful in reproducing the experimental data with appropriate choice of model parameters [9], it does not provide information on how each head in a kinesin molecule works to produce unidirectional motion of the motor. In theories of the second category a motor is viewed as one or a set of Brownian particle(s) moving in a one-dimensional periodic potential representing the interaction between a motor and a track [10–19]. One-particle models are easier to analyze, and not only the motor velocity [10–17,19] but also the detachment process of the motor from the track [18] have been studied. However, one cannot investigate the way the two heads coordinate in processive motion of a motor based on one-particle models. Brownian-particle models with multidegrees of freedom have been introduced based on the hand-over-hand mechanism [12,19] or the inchworm mechanism [13,17] to study the unidirectional motion of kinesin motors, but no attempts seem to have been made to describe the dissociation of motors from microtubules.

The purpose of the present paper is to propose an alternative model of the Brownian-particle type for kinesin motors that allows us to study both the coordination of the motor heads and the detachment process. In our model, a kinesin motor is described as a system consisting of three Brownian particles representing the two heads and a ''hinge'' [13] that is connected to the heads with strings corresponding to ''neck linkers'' [20] in a kinesin molecule. Each head is assumed to behave like a particle in the Brownian ratchet [14,15], since the motility of the single-headed kinesin KIF1A is likely to be explained by this mechanism [21,22], and the thermal detachment process of the head is included in a way described in Ref. [18]. A recent experimental finding [20] of neck-linker ''docking,'' a conformational change of a kinesin molecule, is also taken into account in our model.

The motility and processivity of a molecular motor described by the present model is studied by the numerical simulation. It is found that the dependence of the motor velocity and the run length of the motor along the track on the external force (load) and the ATP concentration obtained here agrees qualitatively with that observed experimentally. Furthermore, it is observed that the heads move in a hand-over-hand fashion rather than an inchworm style, though we have not assumed neither of the mechanisms explicitly.

The paper is organized as follows. Our model is described in the following section. After the method of numerical analysis and the choice of model parameters are explained in Sec. III, we will present the results of simulation and provide qualitative discussion about them in Sec. IV. Section V will be devoted to concluding remarks.

II. MODEL

A. Outline of the model

We consider a simple model, whose structure is schematically shown in Fig. 1, for a two-headed molecular motor,

*Author to whom all correspondence should be addressed. Electronic address: sasaki@nlap.apph.tohoku.ac.jp

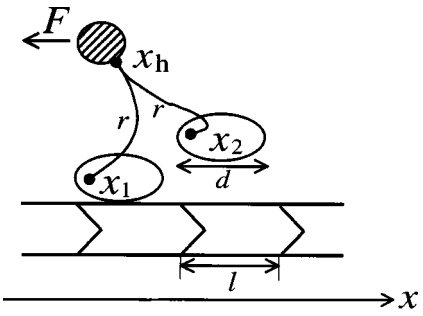

FIG. 1. Schematic representation of the present model for a two-headed kinesin motor. The motor consists of two heads (white ellipses) and a hinge (shaded circle), and each head is connected to the hinge with a string, called a neck linker, of length r. The heads interact with a polar track with a periodic structure of period l. The motor is supposed to move to the right, the forward direction, if no external force F is applied to the hinge. The displacements of the heads and the hinge are represented by the x coordinate with the x axis lying parallel to the track and pointing to the forward direction. A head is treated as a rigid body that makes no rotational motion and has the extent of length d along the track.

kinesin. The system consists of two heads and a hinge. Each head is tethered to the hinge by a ''neck linker,'' a string with certain properties explained below. Here the hinge is assumed to represent the coiled-coil region (neck, stalk, and tail) of kinesin together with a latex bead glued, in the experiments, to the tail; an external load is applied to the bead in an optical-trap experiment. The object consisting of the coiled-coil part of the motor and the bead is treated as a single rigid body, a hinge, for simplicity.

A head can be attached to or detached from the microtubule track. In the attached state a head can move along the track, whereas it undergoes three-dimensional diffusive motion with constraints caused by the neck linker. In the latter case, only the displacement of the head along the track will be considered explicitly in the present model. Similar simplification will be made in describing the motion of the hinge.

Each head in a kinesin motor catalyzes the hydrolysis reaction of ATP into ADP and inorganic phosphate Pi, ATP $\rightarrow$ADP+Pi. The forward reaction is dominant under the condition of high ATP concentration and low ADP concentration, which is realized in the experiments on molecular motors and in living cells. Therefore, we shall ignore the backward reaction in what follows. After the hydrolysis is completed at the nucleotide-binding site on a head, Pi and ADP molecules leave the head sequentially. Hence, a head goes through four chemical states cyclically as

$$\mathrm{K}\rightarrow\mathrm{KT}\rightarrow\mathrm{KDP}\rightarrow\mathrm{KD}\rightarrow\mathrm{K}, \tag{1}$$

where K is the nucleotide-free state (K stands for kinesin without nucleotide), KT or KD is the state with ATP or ADP bound, respectively, and KDP is the state with both ADP and Pi bound. Considering the fact that a head can be attached to or detached from the microtubule track, one may need to take into account at least eight distinct states for each head.

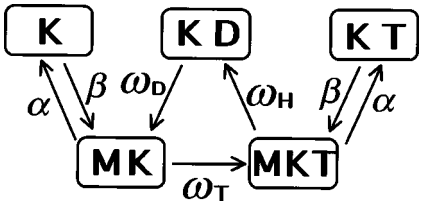

FIG. 2. Five states of a head considered in the present model are represented by the boxed symbols, and the transitions between the states are indicated by the arrows. A head is attached to the track in states MK and MKT, while it is detached in the other states, K, KD, and KT. The symbol accompanying each arrow denotes the associated transition rate.

In order to make the model simple and still capable of describing the processive motion, we shall consider only the five states shown in Fig. 2, i.e., states K, KD, KT, MK, and MKT. In the states labeled with and without symbol M, the kinesin head is attached to and detached from the microtubule. The meanings of the other symbols are the same as those explained earlier except that the two stages, KDP and KD, in chemical cycle (1) is now considered as a single state labeled KD. Since it is known [23] that the affinity of the head with the microtubule is large in states K and KT while it is small in state KD (in simplified notation), we do not take state MKD into account.

Among possible transitions between these five states, only those indicated by the arrows in Fig. 2 will be considered in the present model. In this figure the symbols attached to the arrows represent the rates of the corresponding transitions. The three transitions MK$\rightarrow$MKT, MKT$\rightarrow$KD, and KD $\rightarrow$MK are associated with the chemical cycle of ATP hydrolysis, and hence the reverse processes to these transitions are ignored for the reason explained earlier. Transitions MK$\rightarrow$K and MKT$\rightarrow$KT are thermal activation processes; we shall assume that the affinity of the head to the track is the same in states K and KT, and hence the transition rates of these processes will bear the same value α. Similarly, the same transition rate β will be assigned to the reverse transitions K$\rightarrow$MK and KT$\rightarrow$MKT. Transitions KT$\rightarrow$KD and KD$\rightarrow$K will not be taken into account because the hydrolysis of ATP and the release of ADP proceed very slowly in the absence of microtubule [1]. Transition K$\rightarrow$KT is expected to occur with the rate close to ω_T, since the rate should be determined by how often the head encounters ATP molecules as in the case of transition MK$\rightarrow$MKT. However, the other transition, K$\rightarrow$MK, from state K is likely to proceed much faster and dominates the transition from this state (see Table I below and the Appendix). Therefore we ignore transition K$\rightarrow$KT.

The heads and the hinge undergo translational motion, while each head changes its state through the transitions indicated in Fig. 2. The processive motion of the motor on the track lasts until both the heads become detached. Hence, we are interested in the situation where at least one of the heads is in an attached state, and wish to figure out how long such a situation lasts. The detailed descriptions of the translational motion and the transition rates in our model will be given separately in the following subsections.

TABLE I. The values of the parameters used in the numerical calculation whose results are presented in Figs. 5, and 7–9. The third column indicates the locations in the text where the meanings or the definitions of the parameters are provided.

Parameter	Value	Meaning
l	8 nm	Fig. 1
d	4 nm	Fig. 1
r	2.25 nm	Fig. 1
μ_a	10^4 nm/(pN s)	Eqs. (3), (2a)
μ_d	1.6×10^7 nm/(pN s)	Eqs. (3), (2a)
μ_h	10^5 nm/(pN s)	Eq. (2b)
U_a	$25k_BT$	Fig. 3
a	2 nm	Fig. 3
α_0	0.025 s^{-1}	Eq. (18)
β	5×10^5 s^{-1}	Fig. 2
ω_D	1.1×10^3 s^{-1}	Fig. 2
k_T	2 $(\mu M\,s)^{-1}$	Eq. (17)
Ω_0	1.5 s^{-1}	Eq. (14)
Ω_1	10^4 s^{-1}	Eq. (14)
κ	80 nm^{-1}	Eq. (14)
l_{th}	6.5 nm	Eq. (14)
δ	0.32 nm	Eq. (16)
K	16.46 pN/nm	Eqs. (9), (10)
f	5.66 pN	Eq. (10)

B. Translational motion

Let x_1 and x_2 be the locations of the heads along the track, and x_h be that of the hinge. We assume that these variables change with time according to the following Langevin equations in the overdamped limit [15]:

$$\frac{1}{\mu_{j_n}}\frac{dx_n}{dt}=-\frac{\partial}{\partial x_n}W_{j_1,j_2}+\Gamma_{n,j_n}(t)\quad(n=1,2),\tag{2a}$$

$$\frac{1}{\mu_h}\frac{dx_h}{dt}=-\frac{\partial}{\partial x_h}W_{j_1,j_2}+\Gamma_h(t),\tag{2b}$$

where μ_{j_n} is the mobility of the nth head in state j_n (j_n = K, KD, KT, MK, MKT) and μ_h is the mobility of the hinge; W_{j_1,j_2} is the potential energy of the system when the first and second heads are in states j_1 and j_2, respectively; Γ's are random forces acting on the heads and the hinge. The mobilities of a detached head and the hinge are thought to be determined by the viscosity of the surrounding fluid (water), while the mobility of an attached head is likely to be limited by the "protein friction" [24] arising from the interaction between the head and the track; see the Appendix and Table I. Accordingly, it will be assumed that the mobility of a head is different in attached and detached states, i.e.,

$$\mu_{j_n}=\begin{cases}\mu_a & \text{for } j_n=\text{MK, MKT}\\ \mu_d & \text{for } j_n=\text{K, KD, KT.}\end{cases}\tag{3}$$

The random forces are, as usual, of Gaussian with zero means and and the following variances [25]:

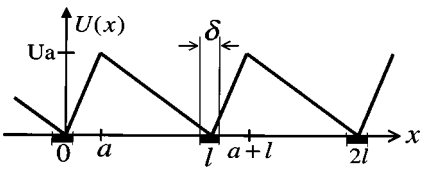

FIG. 3. The potential $U(x)$ representing the interaction between the track and a head in attached states. The transition MKT→KD of a head is possible when it is located in one of the intervals of length δ indicated by the bold lines on the x axis.

$$\langle\Gamma_{n,j_n}(t)\Gamma_{n,j_n}(t')\rangle=(2k_BT/\mu_{j_n})\,\delta(t-t'),\tag{4a}$$

$$\langle\Gamma_h(t)\Gamma_h(t')\rangle=(2k_BT/\mu_h)\,\delta(t-t'),\tag{4b}$$

where the angular brackets indicate the statistical average, k_B is the Boltzmann constant, T is the temperature, and $\delta(t)$ is Dirac's δ function; random forces with different subscripts are statistically independent.

The potential energy W_{j_1,j_2} of the system may be expressed as follows:

$$W_{j_1,j_2}(x_1,x_2,x_h)=U_{j_1}(x_1)+U_{j_2}(x_2)+U_{j_1,j_2}(x_1,x_2)+U_{h,j_1}(x_h,x_1)+U_{h,j_2}(x_h,x_2)+Fx_h,\tag{5}$$

where $U_{j_n}(x_n)$ represents the interaction between the nth head in state j_n and the track, $U_{j_1,j_2}(x_1,x_2)$ the interaction between the heads, $U_{h,j_n}(x_h,x_n)$ the interaction between the hinge and the nth head in state j_n, and Fx_h the potential attributed to the external force (load) F acting on the hinge. The motor is supposed to move towards the plus end of the x axis without the load, and a positive value is assigned to F if the force acts "backwards;" the positive and negative directions of the x axis will be referred to as forward and backward directions, respectively.

We assume that a head interacts with the microtubule only when it is in attached states:

$$U_{j_n}(x_n)=\begin{cases}U(x_n) & \text{for } j_n=\text{MK, MKT}\\ U_d & \text{for } j_n=\text{K, KD, KT,}\end{cases}\tag{6}$$

where U_d is a constant while $U(x)$ should be a periodic and asymmetric function of x, due to the periodicity and polarity of the microtubule structure. A simple piecewise linear function of the sawtooth shape shown in Fig. 3 will be used as $U(x)$, as often used in the literature of Brownian ratchet models [14,15,21,22]. This particular function $U(x)$ is characterized by the potential height U_a, the period l, and the distance a from a potential minimum to the nearest maximum on the right, see Fig. 3. It will be assumed that $0<a<l/2$ (the potential would be symmetric if $a=l/2$).

A head occupies a finite volume in space, and the two heads will not overlap. This excluded-volume effect is represented by U_{j_1,j_2} in Eq. (5). It will be assumed that this effect works only if both the heads are attached to the track, since a detached head is supposed to undergo three-

dimensional Brownian motion, which will not be affected very much by the other head. Thus, we adopt the following expression for the head-head interaction: Let d be the length of a head along the track (see Fig. 1), then

$$U_{j_1,j_2}(x_1,x_2)=+\infty \tag{7a}$$

if $|x_1-x_2|<d$ and both j_1 and j_2 are either MK or MKT, and

$$U_{j_1,j_2}(x_1,x_2)=0 \tag{7b}$$

otherwise.

A head interacts with the hinge through the neck linker. In order to model this interaction, we take into account two effects suggested by the experiments. The first is the so-called neck-linker docking [20]: for a single-headed construct of kinesin it is suggested that the neck linker is fluctuating if the head has no nucleotide or it binds ADP, whereas the linker is held fixed (docked) on the head when ATP is bound. This leads us to assume that the hinge-head interaction depends on the nucleotide state of the head:

$$U_{\mathrm{h},j_n}(x_\mathrm{h},x_n)=\begin{cases} V_0(x_\mathrm{h}-x_n) & \text{for } j_n=\mathrm{K,MK,KD} \\ V_\mathrm{T}(x_\mathrm{h}-x_n) & \text{for } j_n=\mathrm{KT,MKT}, \end{cases} \tag{8}$$

where V_0 and V_T represent the interactions in the undocked and docked states, respectively, and will be specified below.

The second concern about the hinge-head interaction is the length r of the neck linker. It is observed that two-headed kinesin motors take steps of stride l [26]. However, the neck linker is not long enough ($2r<l$) to allow this step size, and it is suggested that the coiled-coil region (represented by the hinge in the present model) needs to be unwound partially when the kinesin moves. We assume that an undocked linker behaves like a flexible string (without elasticity) and that an elastic restoring force acts if the coiled coil is unwound (i.e., if $|x_\mathrm{h}-x_n|>r$). With these assumptions we have

$$V_0(\Delta x)=\begin{cases} 0 & \text{for } |\Delta x|<r \\ \dfrac{1}{2}K(|\Delta x|-r)^2 & \text{for } |\Delta x|>r, \end{cases} \tag{9}$$

where K is the elastic constant associated with unwinding of the coiled coil.

The hinge-head interaction in the docked state, V_T in Eq. (8), will be described as follows. When a head is in states KT or MKT, the head interacts with the neck linker such that it is most stable if the full length r of the linker is docked on the head. However, if the hinge is pulled backwards (towards the negative x direction), by the external load or by the other head, the linker may be "unzipped" partially (see Fig. 4). We suppose that the energy associated with the linker-head interaction increases in proportion to the length of the unzipped portion of the linker. The unwinding of the coiled-coil region may also occur. Let y be the length of the unzipped portions of the linker and u be the length of the unwound coiled coil (see Fig. 4). Then the hinge-head interaction can be expressed as

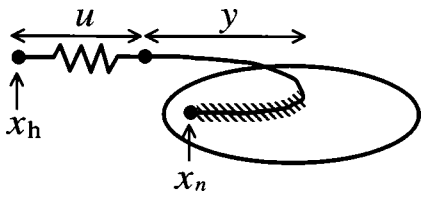

FIG. 4. Partially docked neck linker is represented schematically together with the hinge and the head associated with the linker. The docked portion of the linker is hatched. Here u and y are the lengths of the stretched and unzipped portions of the linker.

$$V_\mathrm{T}=2fy+\tfrac{1}{2}Ku^2, \tag{10}$$

where the parameter $f>0$ represents the strength of the docking, and has the dimensions of force; f will be referred to as the docking force.

We would like to express V_T in Eq. (10) as a function of $\Delta x=x_\mathrm{h}-x_n$, where x_h and x_n are the locations of the hinge and the head, respectively. If the docking is incomplete (see Fig. 4), y is related with Δx and u as $y=(r-\Delta x-u)/2$. The stretch u, in this case, should be determined such that V_T is minimized for given Δx, which results in $u=f/K$. In the case of complete unzipping we have $y=r$ and $u=|\Delta x|-r$, whereas in the case of complete docking we have $y=0$ and $u=|\Delta x-r|$. Thus we obtain, from Eq. (10),

$$V_\mathrm{T}(\Delta x)=f(r-\Delta x)-f^2/2K \tag{11a}$$

for $-r-f/K<\Delta x<r-f/K$ (incomplete docking),

$$V_\mathrm{T}(\Delta x)=2fr+K(\Delta x+r)^2/2 \tag{11b}$$

for $\Delta x<-r-f/K$ (complete unzipping), and

$$V_\mathrm{T}(\Delta x)=K(\Delta x-r)^2/2 \tag{11c}$$

for $\Delta x>r-f/K$ (complete docking).

C. Transition rates

There is experimental evidence that the chemical reactions on the two heads of a motor molecule are coordinated to realize the processive motion of the motor. In other words, some of the transition rates shown in Fig. 2 associated with one head depends on the locations of the heads and/or on the state of the other head.

Consider the situation where one head is attached and the other with ADP bound is detached. It is known [1] that the detached head releases the ADP very slowly if the attached head has no nucleotide, while the binding of ATP to the attached head accelerates the release of ADP from the second head drastically (by about 5000-fold or more). We take this fact into account in a simplified way: the rate ω_D1 of the transition for head 1 from states KD to MK is assumed to be given by

$$\omega_\mathrm{D1}=\begin{cases} \omega_\mathrm{D}\Theta(|x_1-x_2|-d) & \text{if } j_2=\mathrm{MKT} \\ 0 & \text{otherwise}, \end{cases} \tag{12}$$

where ω_D is a constant and the step function Θ, defined by

$$\Theta(x)=\begin{cases}1 & \text{for } x>0\\ 0 & \text{for } x<0,\end{cases} \tag{13}$$

represents the excluded-volume effect of the heads. The expression for ω_{D2}, the corresponding transition rate for head 2, is given by Eq. (12) with subscripts 1 and 2 interchanged.

Transition MKT→KD is another example that is associated with a coordination of the two heads: the detachment of a head associated with the ATP hydrolysis is accelerated drastically by the presence of the other head (one-headed kinesin is detached very slowly), and it is suggested that the attachment of the second head on the microtubule causes intramolecular strain that catalyzes the detachment of the first head [23]. In the present model, we assume that the detachment rate ω_H increases abruptly from a small value Ω_0 to a large one Ω_1 when the distance between the heads (strain) exceeds certain threshold value l_{th}, and express it as follows:

$$\omega_H(x_1-x_2)=\tfrac{1}{2}\{\Omega_0+\Omega_1+(\Omega_1-\Omega_0)\times\tanh[\kappa(|x_1-x_2|-l_{th})]\}, \tag{14}$$

where κ is a parameter.

We make another assumption, proposed by Prost *et al.* [10,15,16,18], on the transition MKT→KD: the hydrolysis reaction of ATP is catalyzed most efficiently when the head is bound at particular sites on the microtubule. Following Prost *et al.* [10,15,16,18] it will be assumed that the ATP hydrolysis and hence the transition MKT→KD takes place when the head is in small intervals of length δ around the minima of the potential $U(x)$ for the head-track interaction. These intervals are indicated by the bold lines on the x axis in Fig. 3. The transition rate for head 1 is expressed as

$$\omega_{H1}(x_1,x_2)=\omega_H(x_1-x_2)\Theta_{loc}(x_1), \tag{15}$$

where the function ω_H is given in Eq. (14), and Θ_{loc} is defined by

$$\Theta_{loc}(x)=\begin{cases}1 & \text{if } U(x)<(\delta/l)U_a\\ 0 & \text{otherwise.}\end{cases} \tag{16}$$

The expression for ω_{H2}, the corresponding transition rate for head 2, is given by Eq. (15) with subscripts 1 and 2 interchanged.

The rest of the transitions shown in Fig. 2, other than the two discussed above, are supposed to take place independently on the two heads. Transition MK→MKT results from the binding of ATP on a head. Hence, the corresponding transition rate ω_T is assumed to be proportional to the ATP concentration [ATP], i.e.,

$$\omega_T=k_T[\mathrm{ATP}], \tag{17}$$

where k_T is a constant. The detachment processes MK→K and MKT→KT as well as their reverse processes are caused by the thermal fluctuation, and it would be reasonable to assume that

$$\alpha=\alpha_0\exp[U(x)/k_BT] \tag{18}$$

with α_0 being a constant and that β is independent of x, the location of the head [18].

III. METHOD OF NUMERICAL ANALYSIS

We integrate the coupled Langevin equations (2) numerically, by taking account of the transition rates discussed in Sec. II C, to analyze the processive motion of the motor in the present model. This Langevin simulation is carried out for a large number of samples, under the following initial condition:

$$j_1=\mathrm{MK},\quad j_2=\mathrm{KD},\quad x_1=x_2=x_h=0 \tag{19}$$

at $t=0$. The simulation for each sample is continued until both the heads become detached (become in states K, KD, or KT). Let τ_i be the time at which the simulation of the ith sample ends, and L_i be the location of the hinge in this sample at this moment. The sample average of τ_i and L_i, denoted by $\langle\tau\rangle$ and $\langle L\rangle$, will be called the *mean run time* and the *mean run length*, respectively. The *mean motor velocity* $\langle v\rangle$ is calculated as a weighted average

$$\langle v\rangle=\sum_{i=1}^{N} v_i w_i,\quad w_i=\tau_i\Big/\sum_{j=1}^{N}\tau_j \tag{20}$$

of sample velocities $v_i=L_i/\tau_i$, where N is the number of the samples and the weight w_i is proportional to τ_i since the variance of v_i is inversely proportional to τ_i. The number of samples used in the actual numerical simulation is $N=100$ for the low ATP concentration of $[\mathrm{ATP}]=5$ μM and $N=100-400$ for the high ATP concentration of $[\mathrm{ATP}]=2$ mM.

Our main interest is the dependence of $\langle v\rangle$, $\langle L\rangle$, and $\langle\tau\rangle$ on the external load F and the ATP concentration [ATP]. Apart from F and [ATP], there are 19 parameters in the present model. Their values are set, unless otherwise stated, as listed in Table I in the numerical analysis such that the results can be compared with experiment on kinesin. The values or the ranges of values for some parameters (e.g., l and μ_d) can be determined more or less directly from experimental facts, while the others (e.g., κ and δ) cannot be assigned *a priori*. The Appendix explains how we have chosen the values of the parameters listed in Table I.

IV. RESULTS AND DISCUSSION

A. Movement of the heads

In Fig. 5(a) we show the trajectories of the two heads obtained in a typical simulation with $F=0$ pN and $[\mathrm{ATP}]=2$ mM. It can be seen that the motor of the present model steps forward with increments of $l=8$ nm. In this figure, each of the vertical arrows indicates a moment when one ATP molecule is hydrolyzed (i.e., transition MKT→KD takes place). It is clearly seen that the ATP hydrolysis is strongly coupled to the 8 nm steps, in agreement with the experiments (with low loads and high ATP concentrations).

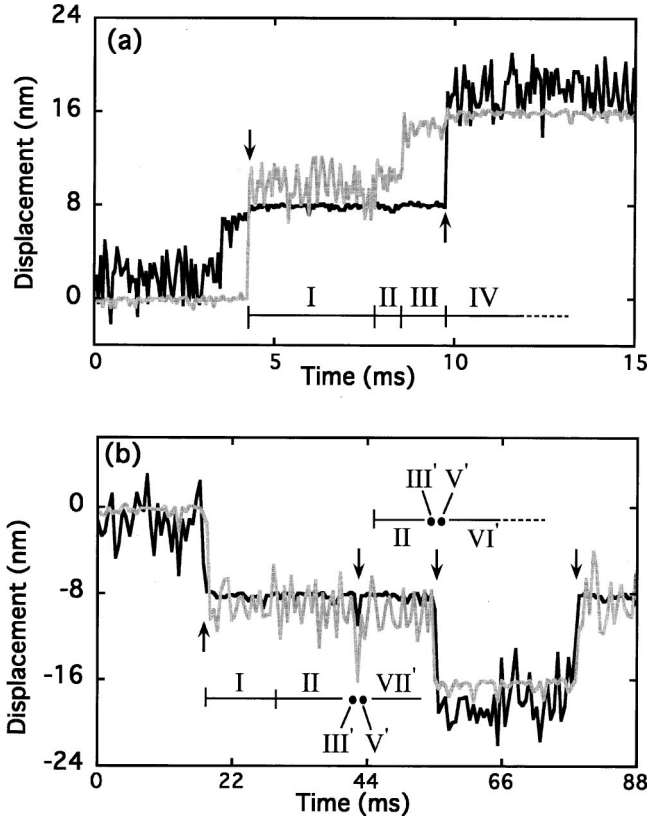

FIG. 5. Parts of the trajectories of the two heads (black and gray lines) obtained in typical simulations with [ATP]=2 mM for (a) $F=0$ pN and (b) $F=7$ pN. The locations of the heads were recorded every 0.057 ms for (a) and 0.57 ms for (b). Each of the vertical arrows indicates the moment when one ATP molecule is consumed. The horizontal line segments labeled I, II, etc. represent the time intervals when the motor is in states I, II, etc., respectively, shown in Fig. 6.

By contrast, the trajectories for $F=7$ pN shown in Fig. 5(b) reveal that the motor often takes backward steps of size 8 nm or moves neither forward nor backward by consuming ATP molecules under the high load.

Let us discuss the movement of the heads and its relation to their chemical states in some detail. For this purpose and other discussions presented below, we refer to Fig. 6, which shows various states of the motor in the present model together with transitions, indicated by the arrows, between them. In this figure the shaded and white circles represent head 1 and head 2, respectively, and a letter inside a circle indicates the chemical state of the corresponding head. For example, in the state labeled I head 1 is in state MK and head 2 is in state KD; state I may change into state Ia with rate $\alpha(x_1)$ or into state II with rate ω_{T}. Note that Fig. 6 presents only a part of all the possible states of the motor, which will be important in our discussion.

When the motor takes one step forward, it changes its state through the path I→II→III→IV shown in Fig. 6 by the wide black arrows; another path II→III→V→VI is also available if the rate ω_{T} is large under high ATP concentrations. State IV (state VI) is equivalent to state I (state II) except that head 1 and head 2 are interchanged and the attached head in state IV (state VI) is located at a distance $l=8$ nm ahead of the site where the attached head in state I (state II) is located. We have indicated in Fig. 5(a) which portions of the trajectories correspond to these states by the horizontal line segments labeled I, II, III, and IV. From this figure, we can understand that the motor in this condition make a forward step of 8 nm not in a ''inchworm'' style but in a ''hand-over-hand'' style.

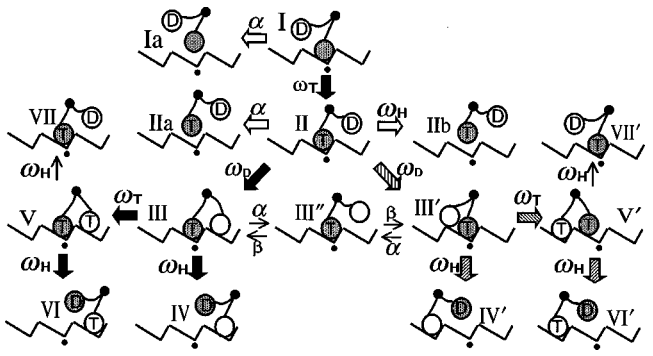

FIG. 6. A part of all the possible states of the motor, which will be important in our discussion, and sequences of transitions between them. The shaded and open circles indicate head 1 and head 2, respectively. The track is represented by the potential profile of Fig. 3, and the dot beneath it indicates the position where the attached head in states I and II is located. The wide black arrows indicate the transitions that occur frequently under the low external force $F\sim 0$. The wide hatched arrows indicate the transitions that lead to backward steps and become important under the high external force $F>f$. The wide open arrows indicate the transitions leading to the detachment of the motor from the track.

When the motor takes one step backward under high loads, it changes its state through the path I→II→III′→IV′ or II→III′→V′→VI′ in Fig. 6. On the other hand, the sequence of transitions II→III′→V′→VII′ leads to a futile process in which the motor returns to the same location after consuming one ATP molecule. The time interval corresponding to these states are indicated by the line segments labeled I, II, III′, etc., in Fig. 5(b).

B. Processivity

The mean run length $\langle L\rangle$ as a function of load F is shown in Fig. 7 for [ATP]=2 mM and [ATP]=5 μM, and the mean run time $\langle\tau\rangle$ is plotted in the inset of Fig. 7. Both run length and run time decrease as the load increases. By contrast, the dependence of these quantities on the ATP concentration has opposite tendency: $\langle L\rangle$ increases while $\langle\tau\rangle$ decreases as [ATP] increases. These properties of the mean run length are also observed experimentally [8]. The calculated value of $\langle L\rangle$ is on the order of the experimental one: in the case of the high ATP concentration of 2 mM, Fig. 7 shows that $\langle L\rangle\sim 600$ nm for $F\sim 0$, which should be compared with $\langle v\rangle\sim 1000$ nm for $F\sim 0$ obtained experimentally by Schnitzer, Visscher, and Block [8]; in the case of the low ATP concentration of 5 μM, we have $\langle L\rangle\sim 200$ nm for $F\sim 0$, while $\langle L\rangle\sim 500$ nm for $F\sim 0$ in the experiment [8].

High processivity is realized under the low load both in our simulation and in the experiment. In order to achieve

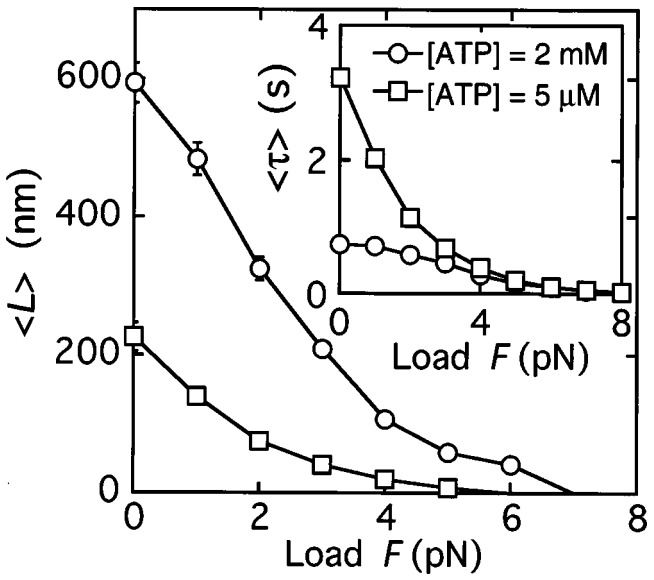

FIG. 7. The mean run length $\langle L\rangle$ as a function of the load F for [ATP]=2 mM and [ATP]=5 μM. Inset: mean run time $\langle\tau\rangle$ as a function of the load F for [ATP]=2 mM and [ATP]=5 μM.

high processivity, the detachment of an attached head should hardly occur when the other head is already detached. This means that the rate of transition I→Ia in Fig. 6 should be much smaller than the rate of transition I→II, and that the rates of transitions II→IIa and II→IIb should be much smaller than the the rate of transition II→III. As explained below, these conditions are realized by the low rate α_0 of thermal detachment from the bottom of the potential valley and by the coordination of the two heads associated with the ATP hydrolysis represented by Eq. (14).

Since the attached head is located near the bottom of the potential valley for $F\sim 0$ because of large potential height $U_a \gg k_B T$, the rates of transitions I→Ia and II→IIa are about $\alpha_0 \sim 10^{-2}$ s^{-1}. This rate is much smaller than the rate of transition I→II, because the latter is as large as $\omega_T \sim 10$ s^{-1} even for the low ATP concentration of 5 μM. The rate α_0 is also much smaller than the rate of transition II →III, which is of the order $\omega_D \sim 10^3$ s^{-1} [27]. Thus, we see that the thermal detachment of the motor is unlikely to occur for $F\sim 0$. Now, according to Eq. (14), the rate of the detachment due to the ATP hydrolysis, II→IIb, is $\Omega_0 \sim 1$ s^{-1} if the distance between the heads in state II is small such that inequality

$$|x_1 - x_2| < l_{\rm th} - 1/\kappa \tag{21}$$

is satisfied, whereas it can be quite large, $\Omega_1 \sim 10^4$ s^{-1}, if the distance is so large that inequality $|x_1 - x_2| > l_{\rm th} + 1/\kappa$ holds. One can deduce from Eq. (5) that in state II the hinge is located at

$$x_{\rm h} = \begin{cases} r - F/K, & F < f \\ -r - F/K, & F > f \end{cases} \tag{22}$$

and the attached head is sitting at $x_1 = 0$ if the thermal fluctuation is neglected. The detached head moves back and forth in the interval of length about $2r$ around the hinge since $\mu_{\rm d} \gg \mu_{\rm h}$. Therefore the distance between the heads in state II is at most

$$|x_1 - x_2| \sim 2r + b\sqrt{k_B T/K} \tag{23}$$

for $F\sim 0$, where the second term on the right-hand side, with b being a factor of order unity, is due to the stretching of the neck linker by thermal fluctuation. With the parameter values listed in Table I, the distance given by Eq. (23) satisfies inequality (21). Thus, we find that the rate of detachment II →IIb is about $\Omega_0 \sim 1$ s^{-1}, which is much smaller than the rate of transition II→III, implying the high processivity.

It is expected from the above discussion that the processivity for $F\sim 0$ will be reduced if K, $l_{\rm th}$, or κ becomes small, since these changes in parameters are unfavorable for inequality (21) being satisfied. We have verified this expectation by numerical simulation (date not shown).

Let us consider the dependence of the mean run length $\langle L\rangle$ on the ATP concentration under the low external load ($F\sim 0$). Let $p_{\rm d}$ be the probability for the motor to leave the track in each cycle of stepping. Then the mean run length can be estimated as

$$\langle L\rangle \sim l/p_{\rm d}, \tag{24}$$

since the detachment occurs approximately once in $1/p_{\rm d}$ steps for $p_{\rm d} \ll 1$ (high processivity). Here, probability $p_{\rm d}$ can roughly be estimated as

$$p_{\rm d} \sim \frac{\tilde{\alpha}}{\omega_{\rm T}} + \frac{\Omega_0 + \tilde{\alpha}}{\tilde{\omega}_D}, \tag{25}$$

where the first term is the contribution from transition I →Ia and the second term from transitions II→IIa and II →IIb. In this equation, $\tilde{\alpha}$ is the rate of thermal detachment (transition I→Ia or II→IIa) and may be approximated by α_0 for $F\sim 0$, and $\tilde{\omega}_{\rm D}$ is the rate of transition II→III, which is different from $\omega_{\rm D}$ due to the excluded-volume effect included in Eq. (12). In state II, the hinge is located at $x_{\rm h} \sim r - F/K$ for $F<f$, as given in Eq. (22) (assuming that the attached head is sitting at $x_1 = 0$), and the detached head moves rapidly in the interval $[x_{\rm h} - r, x_{\rm h} + r]$ of length $2r$, resulting in a uniform distribution of its position. However, this head can be attached to the track only when it is in the interval $[d, x_{\rm h} + r]$ of length $2r - F/K - d$ because of the excluded volume due to the attached head. Therefore, the effective rate of transition II→III is estimated as

$$\tilde{\omega}_{\rm D} \sim \omega_{\rm D} \frac{2r - F/K - d}{2r} \quad \text{for} \quad F\sim 0, \tag{26}$$

which is about one order of magnitude smaller than $\omega_{\rm D}$. We see from Eq. (25) that $p_{\rm d}$ is expected to decrease with increasing [ATP], which explains, together with Eq. (24), the dependence of $\langle L\rangle$ on [ATP] observed numerically (Fig. 7).

The dependence of the mean run time $\langle\tau\rangle$ on the ATP concentration for $F\sim 0$ can be understood in a similar way. Let $k_{\rm ATP}$ be the rate of the ATP hydrolysis cycle, which cor-

responds to the cycle of transitions I→II→III→IV (or the alternative cycle II→III→V→VI in the case of high ATP concentration) in Fig. 6 for $F\sim 0$. Then the mean run time can be estimated as

$$\langle \tau \rangle \sim 1/k_{\mathrm{ATP}} p_{\mathrm{d}}, \tag{27}$$

where p_{d} is the probability of detachment introduced above. For the ATPase rate k_{ATP} we would have

$$\frac{1}{k_{\mathrm{ATP}}} \sim \frac{1}{k_{\mathrm{T}}[\mathrm{ATP}]} + \frac{1}{\tilde{\omega}_{\mathrm{D}}} + \frac{1}{\Omega_1}, \tag{28}$$

where the three terms on the right-hand side are the average lifetimes of states I, II, and III. Considering the values of the parameters listed in Table I, we can neglect $\tilde{\alpha}$ in the second term in Eq. (25) and the last term $(1/\Omega_1)$ in Eq. (28), since $\alpha_0 \ll \Omega_0$ and $\tilde{\omega}_D \ll \Omega_1$. Substituting Eqs. (28) and (25) after making these simplifications into Eq. (27), we obtain

$$\langle \tau \rangle \sim \frac{1}{\Omega_0}\left[1 + \frac{(\Omega_0 - \alpha_0)\tilde{\omega}_{\mathrm{D}}}{\Omega_0 \omega_{\mathrm{T}} + \alpha_0 \tilde{\omega}_{\mathrm{D}}}\right]. \tag{29}$$

The second term in the square brackets in this equation represents the dependence of $\langle \tau \rangle$ on the ATP concentration, since $\omega_{\mathrm{T}} = k_{\mathrm{T}}[\mathrm{ATP}]$. Note that α_0 in the numerator of this term can again be neglected ($\alpha_0 \ll \Omega_0$), and one finds from Eq. (29) that the mean run time decreases with increasing ATP concentration, which explains the dependence of $\langle \tau \rangle$ on [ATP] observed in Fig. 7.

It may be interesting to see whether the crude estimates of $\langle L \rangle$ and $\langle \tau \rangle$ discussed above give the values comparable to the numerical results shown in Fig. 7. Substituting the parameters adopted in Table I into Eqs. (24) and (27), we get the following values for $F=0$: $\langle L \rangle \sim 640$ nm and $\langle \tau \rangle \sim 0.69$ s at [ATP]=2 mM, while $\langle L \rangle \sim 530$ nm and $\langle \tau \rangle = 7.3$ s at [ATP]=5 μM. These values are on the same order of the results of the simulation for $F=0$ (see Fig. 7): $\langle L \rangle \simeq 593$ nm and $\langle \tau \rangle \simeq 0.74$ s at [ATP]=2 mM, while $\langle L \rangle \simeq 230$ nm and $\langle \tau \rangle \simeq 3.2$ s at [ATP]=5 μM. The discrepancy is larger for the low ATP concentration, which is thought to result from the underestimation of the thermal detachment rate $\tilde{\alpha}$ by α_0.

We can guess the dependence of mean run length $\langle L \rangle$ not only on ω_{T} but also on ω_{D} from Eqs. (24) and (25). Since parameter ω_{D} is supposed to decrease with increasing ADP concentration, $\langle L \rangle$ is expected to get smaller as the ADP concentration becomes larger. For example, $\langle L \rangle$ for $F=0$ and [ATP]=2 mM is estimated to change from 640 nm to 290 nm with the decrease in ω_{D} from 1100 s^{-1} to 500 s^{-1}, according to Eq. (24). This tendency was confirmed by the numerical simulation (data not shown): $\langle L \rangle \sim 600$ nm for $\omega_{\mathrm{D}} = 1100\ \mathrm{s}^{-1}$, and $\langle L \rangle \sim 270$ nm for $\omega_{\mathrm{D}} = 500\ \mathrm{s}^{-1}$.

So far, we have considered the processivity under the low load. If the load is increased, the attached head in state I or II in Fig 6 will have larger chance of climbing the potential slope backwards by the thermal fluctuation, and hence the rate of the thermal detachment given by Eq. (18) will increase. This explains the load dependence of the processivity shown in Fig. 7.

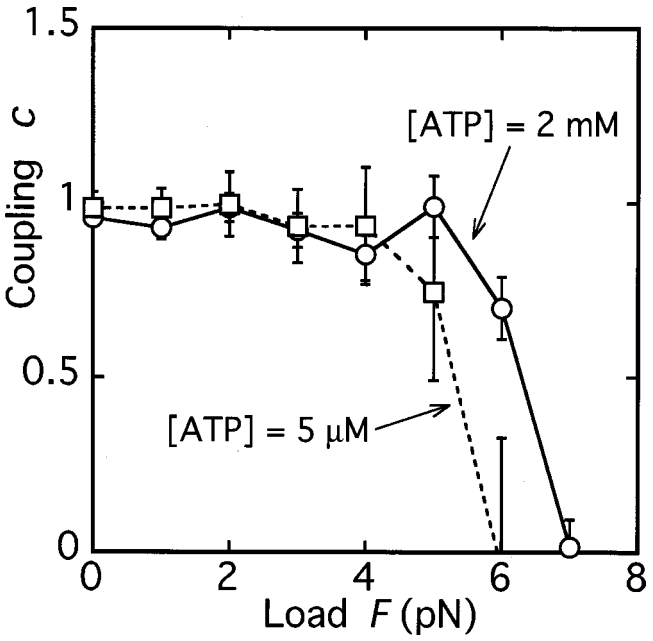

FIG. 8. The mechanochemical coupling parameter c, defined by Eq. (30), as a function of the external load F for [ATP]=2 mM and [ATP]=5 μM.

C. Mechanochemical coupling

The experimental evidence [28,29] indicates that conventional kinesin takes one step forward every time it hydrolyzes one ATP molecule under the condition of low load ($F\sim 0$) and high ATP concentration ([ATP]$\sim$2 mM). In other words, the mechanochemical coupling is tight. Figure 5 suggests that the tight coupling seems realized in the present model for $F\sim 0$, and the tight coupling has been assumed implicitly in the discussion of processivity under low loads in the preceding subsection. In order to measure the degree of mechanochemical coupling in the present model, we define a mechanochemical coupling parameter c by

$$c = \frac{1}{N}\sum_{j=1}^{N} \frac{N_j^{\mathrm{step}}}{N_j^{\mathrm{ATP}}}, \tag{30}$$

where N is the number of samples in the simulation, $N_j^{\mathrm{step}} = L_j/l$ is the number of net steps (the number of forward steps minus that of backward steps) in the jth sample, and N_j^{ATP} is the number of ATP hydrolysis cycles. This coupling parameter is plotted against the load F in Fig. 8. One sees that the coupling is tight ($c\sim 1$) in a wide range of F ($F < 4$–5 pN) irrespective of the ATP concentration. As F is increased beyond this range, the coupling parameter c decreases sharply and becomes zero at a certain value of F at which the motor velocity, to be discussed in the following subsections, vanishes.

In order to achieve the tight coupling in the present model, the motor needs to repeat the cycles of transitions I $\rightarrow$II$\rightarrow$III$\rightarrow$IV or II$\rightarrow$III$\rightarrow$V$\rightarrow$VI in Fig. 6. Departures from these cycles may result in termination of processive movement (by transition I$\rightarrow$Ia, for example), stepping backwards (e.g., II$\rightarrow$III$'\rightarrow$IV$'$), or consuming ATP molecules without taking steps (e.g., V$\rightarrow$VII); the first process was discussed in the preceding subsection and the others will be considered here. It will turn out that the docking phenomenon, the excluded-volume effect of the heads, and the asymmetry of potential $U(x)$ play important roles in realizing the tight coupling under low loads in the present model.

First, we note that the chance of transition II$\rightarrow$III$'$, which may result in a backward step, is quite small for $F\sim 0$. As seen in Eq. (22), the hinge in state II is located about distance r ahead of the attached head, head 1, because of the docking of the linker. Therefore, the detached head, head 2, in this state cannot move to a position more than distance d (excluded length) behind the attached head ($x_2<x_1-d$) unless a fairly large fluctuation in the position of the hinge occurs, whereas it has no difficulty to move forward such that $x_2>x_1+d$, as we have discussed in deriving Eq. (26). Thus, it is seen that the linker docking and the excluded-volume effect make the probability of transition II$\rightarrow$III much larger than that of transition II$\rightarrow$III$'$.

Second, we show that even if transition II$\rightarrow$III$'$ happens to take place it will not result in destruction of the tight coupling for $F\sim 0$ [30]. The asymmetry of potential $U(x)$ ensures that the detached head in state II of Fig. 6, head 2, will fall in the valley of potential $U(x)$ where the other head (head 1) sits rather than the left valley next to it when head 2 is attached to the track as a result of transition II$\rightarrow$III$'$. Head 2 in state III$'$ tends to sit near $x_2=-d$ because of the slope of potential $U(x)$ and the excluded-volume effect. This fact implies that state III$'$ is quickly transformed into state III$''$ by thermal activation with the rate of about $\alpha(-d)\sim 4\times 10^5$ s^{-1}, which is much larger than the rates of the other possible transitions from state III$'$: the rate of transition to IV$'$ [31] is estimated from Eq. (15) to be $\omega_{\mathrm{H1}}(0,-d)\sim\Omega_0\sim 1.5$ s^{-1}, that to state V$'$ is at most $\omega_{\mathrm{T}}\sim 4\times 10^3$ s^{-1} even at high ATP concentration of 2 mM, and the detachment of head 1 by thermal activation (this process is not shown in Fig. 6) occurs with rate $\alpha_0\sim 10^{-2}$ s^{-1}. Now the thermally detached head in state III$''$ will be reattached with the high rate of $\tilde{\beta}\sim\beta(2r-d)/2r\simeq 6\times 10^4$ s^{-1}, converting the motor into state III, where the rate $\tilde{\beta}$ is estimated as in the case of $\tilde{\omega}_{\mathrm{D}}$ in Eq. (26); note that transition III$''\rightarrow$III$'$ is unlikely to occur for $F\sim 0$ for the same reason explained above why transition II$\rightarrow$III$'$ is unlikely to occur. If state III is realized, the thermal detachment of head 2 (transition III$\rightarrow$III$''$) hardly occurs because the rate of this transition is as small as $\alpha(x_2)\sim 1$–100 s^{-1}, compared to $\tilde{\beta}$, which is estimated from

$$x_2\sim 2r+2U_{\mathrm{a}}/[K(l-a)]\pm\sqrt{2k_{\mathrm{B}}T/K}, \tag{31}$$

for $F\sim 0$; this equation comes from the consideration of force balance and the thermal fluctuation based on Eq. (5). From these arguments, it can be concluded that state III$'$ is transformed effectively into state III under the low load, leaving little possibility of taking a backward step or resulting in a futile process from state III$'$.

Third, we consider another path leading to the reduction of coupling parameter: transition from state V to state VII in Fig. 6 triggered by the hydrolysis of an ATP molecule on head 2 rather than head 1. Note that state VII is identical with state II, and therefore after the sequence of transitions II$\rightarrow$III$\rightarrow$V$\rightarrow$VII the motor returns to the same position even though one ATP molecule is consumed. However, the transition V$\rightarrow$VII is unlikely to occur, as explained as follows. The rate of this transition is given by $\omega_{\mathrm{H2}}(x_2,x_1)$, which is defined by Eq. (15) with subscripts 1 and 2 interchanged. This rate is zero, due to the factor $\Theta_{\mathrm{loc}}(x_2)$, unless head 2 is located very close to the potential minimum at $x=l$, such that the condition

$$l-x_2<(l-a)\,\delta/l \tag{32}$$

is satisfied. Due to the asymmetry of potential $U(x)$ and limited lengths of the linkers, the rear head (head 1) tends to sit near the bottom of the potential valley ($x_1\sim 0$), while the front head (head 2) is pulled backwards against the potential slope away from the bottom. The location of head 2, x_2, in state V as well as state III can be evaluated by Eq. (31), and the left-hand side of inequality (32) is estimated to be in the range 0.71–2.12 nm with the parameter values in Table I, while the right-hand side of this inequality is calculated to be 0.24 nm. Thus, we find that condition (32) is not satisfied and therefore the transition V$\rightarrow$VII is unlikely to occur.

The above arguments explain how the tight mechanochemical coupling is realized in the present model with parameters listed in Table I under low loads irrespective of the ATP concentration. Furthermore, the discussion associated with inequality (32) implies that the mechanochemical coupling parameter c for $F\sim 0$ will decrease if δ is increased, K is decreased, or r is increased. The amount of decrease in c is expected to be larger for the high ATP concentration than for the low ATP concentration, because the frequency of the transition III$\rightarrow$V, which can result in the reduction of c by transition V$\rightarrow$VII, gets larger as the ATP concentration gets larger. We have carried out numerical simulations by changing the values of these parameters and have actually observed these tendencies (data not shown). For example, the coupling parameter c for $F=0$ is found to change from 0.96 to 0.73, as the neck-linker length r is increased from 2.25 nm to 2.75 nm.

Let us turn our attention to the dependence of the coupling parameter on the load. Under the low load ($F\sim 0$), the main pathways of the transitions are I$\rightarrow$II$\rightarrow$III$\rightarrow$IV or II$\rightarrow$III$\rightarrow$V$\rightarrow$VI, as described above. But, if the external force F gets larger than the docking force f, the position of the hinge in state II is shifted backward [see Eq. (22)]. Therefore, with the increase in F, the probability of transition II$\rightarrow$III$'$ gets larger and that of transition II$\rightarrow$III becomes smaller. If the rear head (head 2) in state III$'$ is attached in the potential valley where the front head (head 1) is sitting, the motor is transformed quickly into state III through thermal detachment III$'\rightarrow$III$''$ and reattachment III$''\rightarrow$III of head

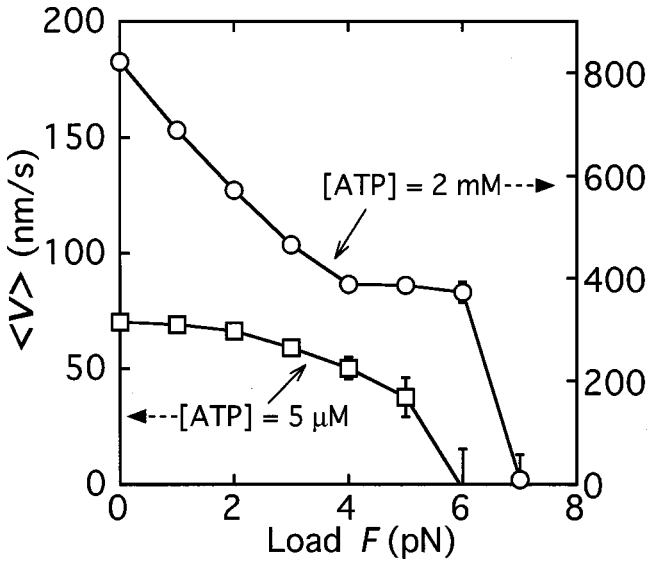

FIG. 9. Load-velocity profiles under the two ATP concentrations, [ATP]=2 mM and [ATP]=5 μM. Note that different scales of the velocity are used in the two cases.

2, as discussed above. However, there are such occasions for large F that head 2 is attached in the left valley next to that where head 1 is located. In this case, transition III$'\rightarrow$III$''$ is unlikely to occur, because head 2 (rear head) tends to sit at the bottom of the valley, where the rate of thermal detachment is quite small ($\alpha_0 \sim 10^{-2}$ s^{-1}), due to the asymmetry of potential $U(x)$ as explained before. Therefore, transitions III$'\rightarrow$IV$'$ and III$'\rightarrow$V$'$ can take place under high loads. As a result, the frequency for the motor to make backward steps increases with the external force. Thus, we expect that the coupling parameter gets smaller as the external force becomes larger, which is what we see in Fig. 8.

D. Velocity

The dependence of the mean velocity $\langle v \rangle$ on the load F (the force-velocity curve) for two choices of ATP concentration, [ATP]=2 mM and [ATP]=5 μM, is shown in Fig. 9. The velocity decreases with increasing F, and becomes zero at a certain value of the load, which is called a *stall force* F_s; the velocity is negative for the load beyond the stall force. Note that the mean run length and the coupling parameter, shown in Figs. 7 and 8, also vanish at the stall force. The force-velocity curves in Fig. 9 agree qualitatively with those obtained experimentally by Visscher, Schnitzer, and Block [7,8]: the stall force as well as the velocity grows with ATP concentration. This dependence of the stall force on ATP concentration was not clearly shown by the earlier theories that take the two-headed structure of kinesin into account explicitly [12,13,17]. Although we have not tried to adjust the model parameters so that quantitative agreement between the theory and the experiment is achieved, the values of the velocity and the stall force are not very far from those of the experiment: in the case of the high ATP concentration of 2 mM, Fig. 9 shows that $\langle v \rangle \sim 800$ nm/s for $F \sim 0$ and $F_s \sim 7$ pN, which should be compared with $\langle v \rangle \sim 800$ nm/s for $F \sim 0$ and $F_s \sim 7$ pN obtained experimentally by Visscher, Schnitzer, and Block [7,8]; in the case of the low ATP concentration of 5 μM, we have $\langle v \rangle \sim 70$ nm/s for $F \sim 0$ and $F_s \sim 6$ pN, which should be compared with $\langle v \rangle \sim 60$ nm/s for $F \sim 0$ and $F_s \sim 5.5$ pN in the experiment.

Roughly speaking, the mean velocity $\langle v \rangle$ of the motor is in proportion to the ATPase rate k_{ATP}:

$$\langle v \rangle \sim c l k_{\mathrm{ATP}}, \tag{33}$$

where c is the mechanochemical coupling parameter, defined by Eq. (30), and l is the step size (the period of the track). Since the coupling is tight ($c \sim 1$) in the wide range of the load, $F < 4$ pN (see Fig. 8), the dependence of the velocity on the load in this range seen in Fig. 9 should reflect the dependence of the ATPase rate on the load. If the coupling is tight, the ATPase rate can be estimated by Eq. (28) with Eq. (26). The force-velocity curve of Fig. 9 for small F can be understood qualitatively from Eq. (33) with $c=1$ together with Eqs. (28) and (26). The first term in Eq. (28) explains the dependence of $\langle v \rangle$ on the ATP concentration: as [ATP] is increased, k_{ATP} and $\langle v \rangle$ increase. The second term in Eq. (28) together with Eq. (26) account for the load dependence: as F is increased, $\tilde{\omega}_{\mathrm{D}}$ decreases and hence $\langle v \rangle$ becomes smaller.

Note that the load dependence of $\langle v \rangle$ is more profound at higher [ATP] in Fig. 9: $\langle v \rangle$ at $F=4$ pN is about half of $\langle v \rangle$ at $F=0$ for [ATP]=2 mM, while $\langle v \rangle$ at $F=4$ pN amounts to 70% of $\langle v \rangle$ at $F=0$ for [ATP]=5 μM. This tendency may be explained by Eq. (28). At high ATP concentrations the second term in Eq. (28) is dominant, and the change in $\tilde{\omega}_{\mathrm{D}}$ resulting from variation of F affects k_{ATP} more strongly than in the case of low ATP concentration where the first term in Eq. (28) is dominant.

It may be worth noting that the crude estimate of the ATPase rate k_{ATP} given in Eq. (28) with Eq. (26) yields reasonable values of velocity for $F \sim 0$. Substituting the parameters listed in Table I to these equations, we obtain the following values from Eq. (33) with $c=1$ for $F=0$: $\langle v \rangle \sim 940$ nm/s at [ATP]=2 mM and $\langle v \rangle = 74$ nm/s at [ATP] =5 μM. Compare these values with the corresponding results of the simulation (see Fig. 9): $\langle v \rangle \simeq 820$ nm/s at [ATP]=2 mM and $\langle v \rangle \simeq 70$ nm/s at [ATP]=5 μM.

The rough estimate of the mean velocity $\langle v \rangle$ by Eq. (33) with Eqs. (28) and (26) enables us to predict the dependence of the velocity on other parameters. For example, under the low external force ($F \simeq 0$), the mean velocity becomes larger (especially at the high ATP concentration), as the neck-linker length r or the transition rate ω_{D} is increased. Actually, we have confirmed this tendency by the numerical simulation and obtained the following results: as ω_{D} is decreased from 1.1×10^4 s^{-1} to 5×10^2 s^{-1}, $\langle v \rangle$ for $F=0$ gets smaller from 823 nm/s to 376 nm/s. As r is increased from 2.25 nm to 2.5 nm, $\langle v \rangle$ becomes larger from 823 nm/s to 1305 nm/s. These values are not too far from those obtained from Eq. (33) with Eqs. (28) and (26).

The dependence of the mean velocity $\langle v \rangle$ on the load F in a range near the stall force F_s is not so easy to understand in contrast to the case of low loads. There seems to be no

simple way of estimating the mechanochemical coupling parameter c and the ATPase rate k_{ATP} when the coupling is no longer tight, because the motor takes various pathways of transition sequences leading to forward steps, backward steps, and futile consumption of ATP molecules in such a circumstance. Although we can understand qualitatively, as discussed in Sec. IV C, that the coupling parameter c decreases with increasing F for large F, we are unable to estimate how fast it decreases. As for k_{ATP}, it is difficult to predict even the tendency whether k_{ATP} increases or decreases if F gets larger around $F \sim F_{\mathrm{s}}$. Numerical simulations (data not shown) reveal that as F is increased k_{ATP} decreases for $F<5$ pN but increases for $F>5$ pN in the case of high ATP concentration of 2 mM. We have not understood this behavior quite well, but the increase in k_{ATP} for large F seems responsible for the appearance of the ''shoulder'' around $F \sim 5$ pN in the force-velocity curve for $[\mathrm{ATP}]=2$ mM in Fig. 9. By contrast, we find numerically that k_{ATP} decreases monotonically with increasing F but it varies very slowly in the case of $[\mathrm{ATP}]=5\ \mu$M. In both of the high and low ATP concentrations, the rapid decrease in c observed in Fig. 8 for $F \sim F_{\mathrm{s}}$ is likely to explain the behavior of the force-velocity curve of Fig. 9 near the stall force.

E. Stall force

As we have pointed out in the preceding subsection, the stall force in the present model increases with the ATP concentration. This tendency may be explained as follows. Consider the system in the ''stalling condition'' in which backward steps occur as frequently as forward steps. Let us ask whether the velocity of the motor will increase or decrease from zero, if the ATP concentration is increased while the other parameters are held fixed; the increase (decrease) in the velocity under this circumstance implies the increase (decrease) in the stall force, because $d\langle v\rangle/dF<0$ in the stalling condition. The increase in [ATP] results in the increase in the rate ω_{T} of ATP binding, and transition $\mathrm{III}' \rightarrow \mathrm{V}'$ seems to be most influential on the velocity among other ATP binding processes. The increase in the rate of transition $\mathrm{III}' \rightarrow \mathrm{V}'$ implies the decrease in the probability of transition $\mathrm{III}' \rightarrow \mathrm{IV}'$; the former transition may result in either a backward step ($\mathrm{V}' \rightarrow \mathrm{VI}'$) or a futile process ($\mathrm{V}' \rightarrow \mathrm{VII}'$), while the latter leads only to a backward step under the high loads. Hence, backward steps occur less frequently as the ATP concentration is increased, which explains the dependence of the stall force on [ATP] observed numerically.

The docking force f seems essential for the model to produce the value of the stall force comparable to the experimental one. We have found (data not shown) that F_{s} is only about 4 pN for $[\mathrm{ATP}]=2$ mM if $f=0$, and that F_{s} increases with f. The reason why F_s is an increasing function of f can be understood as follows. In the stalling condition the transitions from state II to state III and to state III$'$ occur with comparable probabilities. It is not difficult to see that the average location of the hinge in state II shifts towards forward direction if f is increased, even though the stable position without the thermal fluctuation is independent of f: $x_{\mathrm{h}} = -r - F/K$, see Eq. (22). Therefore, if f is increased, the probability of transition II$\rightarrow$III will increase, which results in the increase in velocity from zero; this implies the enhancement of the stall force.

V. CONCLUSION

We have constructed a model for two-headed molecular motors that can describe how the two heads coordinate to produce processive motion and can explain various experimental results qualitatively. From the numerical simulation of the model, demonstrating that the motor in our model moves in a hand-over-hand fashion, the following results associated with motility and processivity of the motor have been obtained: (1) the motor moves by taking one step each time one ATP molecule is hydrolyzed (tight mechanochemical coupling) under low loads; (2) the mean run length decreases with increasing load, whereas it becomes larger with increase in the ATP concentration; (3) the mean run time decreases with increasing load and with increasing ATP concentration; (4) the velocity of the motor decreases with increasing load because the ATPase rate decreases for low loads and the mechanochemical coupling parameter decreases for high loads near the stall force; (5) the stall force increases with ATP concentration. Results (1), (2), and (5) agree qualitatively with what have been observed for two-headed kinesin motors experimentally [7,8,28,29], and the other results, (3) and (4), are hoped to be tested by future experiments.

The dependence of various quantities characterizing the motility of the motor on the model parameters have also been investigated numerically and based on intuitive arguments. Here we note, among others, the dependence on the rate ω_{D} of ADP release and the length r of the neck linker, because these parameters can be controlled experimentally (i.e., ω_{D} by changing the ADP concentration and r by mutation). It is found that the mean run length and the mean velocity decreases but the mean run time changes little when ω_{D} is increased; the mean velocity increases but the mechanochemical coupling parameter decreases when r is increased.

In the present model, it is supposed that the free energy released by the ATP hydrolysis is used to drive the transition of a motor head from the attached state to the detached state, not to translocate the motor directly. The force that drives the motor to move against the viscous environment and external loads is provided mainly by the slope of the asymmetric sawtooth potential for a head attached to the track. Nevertheless, the coupling between the stepping movement of the motor and the ATP hydrolysis reaction results at low loads from the combined effects of the asymmetry of the potential, the head-linker interaction, and coordination of the two head, as explained in Sec. IV C.

Although we have demonstrated that the present model explains various experimental results qualitatively, it should be noted that the model is based on several assumptions for which we do not have clear evidence yet. They include the asymmetric sawtooth potential, the interaction between a head and a neck linker (the docking effect) expressed by the first term in Eq. (10), the effects of a head on the chemical

reaction occurring on the other head (coordination of the heads) represented by Eqs. (12) and (14), and the assumption that the hydrolysis of ATP on a head is possible only when the head is located at particular sites on a microtubule. Much theoretical and experimental efforts need to be made to clarify the validity of the present model as well as to get better understanding of the mechanism of molecular motors.

ACKNOWLEDGMENTS

We would like to express our sincere thanks to Professor F. Matsubara, Professor H. Higuchi, and Dr. T. Nakamura for valuable discussions. One of us (R.K.) acknowledges the financial support of the JSPS Research Fellowships for Young Scientists.

APPENDIX: VALUES OF PARAMETERS

We shall explain how the values of the parameters listed in Table I have been chosen. The structural data of the microtubule and the kinesin provide information on the period l of potential $U(x)$, the length d of a head and the length r of a neck linker. The period of the microtubule 8 nm should be identified with l. The size of a kinesin head is reported to be about $4.5\times4.5\times7$ nm^3 [1] and $3\times3\times9$ nm^3 [13], from which we set $d=4$ nm [17]. The neck-linker region of kinesin is not clearly defined, and its length is estimated to be 2–4 nm [32,33]; the value of r in Table I is in this range.

The mobilities μ_{d} and μ_{h} of a detached head and the hinge, respectively, may be estimated from the Stokes law, by assuming that they are spherical objects moving in water (aqueous solution). The sphere corresponding to the head is assumed to have the same volume as the head, and hence radius of 3 nm is used to obtain the value of μ_{d} in Table I. The hinge in the present model represents the coiled-coil part of kinesin together with a bead attached to it in the experiment. Since the bead is the largest component, the diameter of which is typically 1 μm, the mobility of the hinge can be approximated by that of the bead. The value of μ_{h} in Table I is close to the mobility of a sphere of radius 0.5 μm. The mobility μ_{a} of an attached head can be much smaller than μ_{d}, since the ''protein friction'' [24] arising from the interaction between the head and the microtubule track is expected to be much larger than the viscous drag from the surrounding fluid. The mobility due to the protein friction may be estimated from the observed Brownian motion of a one-headed kinesin KIF1A along a microtubule when ADP is bound on KIF1A [21,22]. From the diffusion constant $D\sim4\times10^4$ nm^2/s obtained from this observation, the mobility is estimated to be about 10^4 nm/(pN s) according to the Einstein relation. We adopt this value μ_{a}, since the structure of the head of KIF1A is similar to that of conventional kinesin considered in this work.

We have little information on the shape of the potential $U(x)$ for the head in attached state other than its periodicity. We suppose that the potential height U_{a} is comparable to the chemical energy of about $20\,k_{\mathrm{B}}T$ released by the hydrolysis of one ATP molecule. For the distance a from a potential minimum to the nearest potential maximum, we choose the value $a=2$ nm, which is nearly equal to that used by Prost *et al.* [10,15,16,18].

Parameter α_0 represents the detachment rate of a head by thermal fluctuation when it is located at a most stable site on the track. We guess that α_0 is of the same order of magnitude as the detachment rate α_0' of a single-headed kinesin, constructed from two-headed kinesin by truncation, with an unhydrolyzable ATP analog (AMP-PMP) bound on it; the single-headed kinesin with AMP-PMP is known to bind strongly on the microtubule at particular sites corresponding, perhaps, to the minima of $U(x)$. The value of α_0 we use is comparable to $\alpha_0'\sim0.01$ s^{-1} obtained experimentally [23].

The rate β of attachment of a detached head to the track may be estimated as follows. Roughly speaking, a detached head undergoes free diffusion inside the spherical region of radius $2r$ around the attached head until it encounters the track. Accordingly, we would have $1/\beta=1/\beta_1+1/\beta_2$, where $1/\beta_1$ is the average time the detached head spends before the encounter and β_2 is the transition rate for the head in the vicinity of the track to be attached to it. The encounter rate can be estimated as $\beta_1\sim2\mu_{\mathrm{d}}k_{\mathrm{B}}T/(2r)^2$, which yields $\beta_1\sim10^6$ s^{-1} with the adopted values for μ_{d} and r. The attachment rate β_2 must satisfy the relation of the detailed balance

$$\beta_2/\alpha=\exp\{[U_{\mathrm{d}}-U(x)]/k_BT\}, \tag{A1}$$

where U_{d} is the potential value in the detached state. It would be reasonable to assume that $U_{\mathrm{d}}>\max_x U(x)$, then we have $\beta_2>10^9$ s^{-1} from relations (A1) and (18) with α_0 and U_{a} adopted above. Thus, it turns out that $\beta_1\ll\beta_2$, and therefore $\beta\simeq1/\beta_1$; the value of β in Table I is consistent with this estimate.

Parameters ω_{D}, k_{T}, and Ω_0 are related with the chemical reactions occurring on a head. Information on these parameters is available from experiments on the kinetic behavior of kinesin motors. For a single-headed construct of conventional kinesin, the rate of ADP release was observed to be about 300 s^{-1} [34,35], which is on the order of ω_{D} we chose. The experimental data on the attachment rate of ATP [34,35] indicates that $k_{\mathrm{T}}\sim2.0\,(\mu\mathrm{M\,s})^{-1}$, and we adopted this value for k_{T}. Parameter Ω_0 is considered to be the rate of ATP hydrolysis on a head in the absence of coordination with the other head, and hence it should be comparable to the hydrolysis rate of about 3.0 s^{-1} observed for a single-headed construct of kinesin; the value of Ω_0 in Table I is consistent with this observation.

Little experimental information is available for the other parameters Ω_1, κ, l_{th}, δ, K, and f. We adopt the value used by Parmeggiani *et al.* [18] for δ, the range of an interval on the track where a head can hydrolyze an ATP molecule. We have decided the values of the remaining five parameters, after carrying out a number of numerical simulations, such that the motor velocity under the low load ($F\simeq0$ pN) and the stall force are on the order of those measured in the experiment by Visscher, Schnitzer, and Block [7,8].

[1] J. Howard, *Mechanics of Motor Proteins and the Cytoskeleton* (Sinauer Associates, Sunderland, MA, 2001).
[2] B. Alberts, A. Johnson, J. Lewis, M. Raff, K. Roberts, and P. Walter, *Molecular Biology of the Cell*, 4th ed. (Garland Science, New York, 2002).
[3] R.D. Vale and R.A. Milligan, Science **288**, 88 (2000).
[4] W. Hua, J. Chung, and J. Gelles, Science **295**, 844 (2002).
[5] K. Svoboda and S.M. Block, Cell **77**, 773 (1994).
[6] H. Kojima, E. Muto, H. Higuchi, and T. Yanagida, Biophys. J. **73**, 2012 (1997).
[7] K. Visscher, M.J. Schnitzer, and S.M. Block, Nature (London) **400**, 184 (1999).
[8] M.J. Schnitzer, K. Visscher, and S.M. Block, Nat. Cell Biol. **2**, 718 (2000).
[9] M.E. Fisher and A.B. Kolomeisky, Proc. Natl. Acad. Sci. U.S.A. **98**, 7748 (2001).
[10] J. Prost, J.-F. Chauwin, L. Peliti, and A. Ajdari, Phys. Rev. Lett. **72**, 2652 (1994).
[11] R.D. Astumian and M. Bier, Phys. Rev. Lett. **72**, 1766 (1994).
[12] C.S. Peskin and G. Oster, Biophys. J. **68**, 202s (1995).
[13] I. Derényi and T. Vicsek, Proc. Natl. Acad. Sci. U.S.A. **93**, 6775 (1996).
[14] R.D. Astumian, Science **276**, 917 (1997).
[15] F. Jülicher, A. Ajdari, and J. Prost, Rev. Mod. Phys. **69**, 1269 (1997).
[16] A. Parmeggiani, F. Jülicher, A. Ajdari, and J. Prost, Phys. Rev. E **60**, 2127 (1999).
[17] G.N. Stratopoulos, T.E. Dialynas, and G.P. Tsironis, Phys. Lett. A **252**, 151 (1999).
[18] A. Parmeggiani, F. Jülicher, L. Peliti, and J. Prost, Europhys. Lett. **56**, 603 (2001).
[19] R.F. Fox and M.H. Choi, Phys. Rev. E **63**, 051901 (2001).
[20] S. Rice *et al.*, Nature (London) **402**, 778 (1999).
[21] Y. Okada and N. Hirokawa, Science **283**, 1152 (1999).
[22] Y. Okada and N. Hirokawa, Proc. Natl. Acad. Sci. U.S.A. **97**, 640 (2000).
[23] W.O. Hancock and J. Howard, Proc. Natl. Acad. Sci. U.S.A. **96**, 13 147 (1999).
[24] K. Tawada and K. Sekimoto, J. Theor. Biol. **150**, 193 (1991).
[25] R. Zwanzig, *Nonequilibrium Statistical Mechanics* (Oxford University Press, Oxford, 2001).
[26] K. Svoboda, C.F. Schmidt, B.J. Schnapp, and S.M. Block, Nature (London) **365**, 721 (1993).
[27] In reality, the rate of transition II→III is about one order of magnitude smaller than ω_D, as discussed in what follows [see Eq. (26)], but is still much larger than α_0.
[28] W. Hua, E.C. Young, M.L. Fleming, and J. Gelles, Nature (London) **388**, 390 (1997).
[29] M.J. Schnitzer and S.M. Block, Nature (London) **388**, 386 (1997).
[30] The consideration in this paragraph ensures that the tight coupling can be realized even if the docking effect is absent ($f=0$) in the present model. Note that transition II→III′ occurs as frequently as transition II→III for $F\sim 0$ if $f=0$, while the former transition rarely occurs as discussed in the previous paragraph if f is positive and not too small.
[31] Here, in state IV′ head 2 (attached head) should sit in the potential valley marked by the dot in Fig. 6 rather than the left valley, since head 2 is located in the former valley in state III′ for $F\sim 0$, as explained above. The situation of state IV′ depicted in Fig. 6 is realized under high loads, which will be discussed later.
[32] E.P. Sablin, Curr. Opin. Cell Biol. **12**, 35 (2000).
[33] M. Tomishige and R.D. Vale, J. Cell Biol. **151**, 1081 (2000).
[34] S.P. Gilbert, M.L. Moyer, and K.A. Johnson, Biochemistry **37**, 792 (1998).
[35] M.L. Moyer, S.P. Gilbert, and K.A. Johnson, Biochemistry **37**, 800 (1998).